Aggregate defects of gold and platinum with lithium in silicon: I. Magnetic resonance investigations

P. Alteheld, S. Greulich-Weber, J.-M. Spaeth, H. Weihrich, and H. Overhof
Fachbereich Physik, Universität-GH Paderborn, D-33095 Paderborn, Federal Republic of Germany

M. Höhne
Institut für Kristallzüchtung, Rudower Chaussee 6, D-12489 Berlin, Federal Republic of Germany
(Received 17 January 1995)

Trigonal and orthorhombic Au (Pt) defects in Si additionally doped with Li and P, previously investigated with electron paramagnetic resonance (EPR), are shown to be aggregate defects involving substitutional Au (Pt) and interstitial Li. The small Li hyperfine interactions, not resolved in EPR, could be measured with electron nuclear double resonance (ENDOR). With double ENDOR it is established that the trigonal defects consist of Au_{Si}-Li_3 (Pt_{Si}-Li_3) aggregates, while the orthorhombic defects are Au_{Si}-Li (Pt_{Si}-Li) pair defects. For the trigonal defects the Li hyperfine interaction matrices are asymmetric. The smallness of the Li hyperfine interaction suggests ionic bonding between the interstitial Li ions and the substitutional Au_{Si} (Pt_{Si}) atoms.

I. INTRODUCTION

Au is one of the most common elements in Si technology used for electrical contacts. Substitutional Au (and Pt) point defects act as effective recombination centers. In special devices, these centers are intentionally incorporated for the control of the lifetime of charge carriers. In most other devices, these centers degrade the performance and there is a need for gettering or passivation processes that reduce the number of Au centers, forming Au (Pt) aggregate defects. Several pair defects involving interstitial $3d$ transition metals, such as Au_{Si}-Fe_i, Au_{Si}-Mn_i, and Au_{Si}-Cr_i have been investigated with electron paramagnetic resonance[1–3] (EPR). These centers, however, are not suitable as gettering centers, because they have states in the gap.

One process for removing the detrimental effect of Au is the P-Au gettering. Since it was reported that the gettering process is more effective at a higher position of the Fermi level, Si was additionally diffused with Li. Isolated Li induces a shallow donor level at E_{CB}-0.034 eV.[4] After Li in-and-out diffusion, the EPR of a trigonal "Si-Au pair" defect[4] with a resolved hyperfine (hf) structure, due to ^{29}Si and ^{197}Au was observed. In the EPR spectrum, no hf signature neither of ^{31}P nor of ^{6,7}Li was observed. A similar process involving Pt instead of Au later led to the detection of the "Si-Pt pair."[5]

In the same sample where the trigonal defects were detected, we subsequently discovered the presence of another type of Au (Pt)-related defects with orthorhombic symmetry when measuring the EPR at temperatures below 10 K. These defects also revealed an hf interaction (hfi) with ^{197}Au and ^{29}Si and could, therefore, be assigned to another Au (Pt)-Si pair defect. The question arose whether Au (Pt)-Si pairs have metastable properties in analogy to, e.g., Al-Fe pairs.[6–9]

If either P or Li were involved in the formation of the trigonal and orthorhombic "pair defects," then the resolution of further hf interactions (hfi) should help to get more information on the microscopic structures of these defects. We, therefore, performed electron nuclear double resonance (ENDOR) experiments, in which small hfi could be resolved. We show that both the trigonal and orthorhombic defects of Au as well as Pt involve Li as part of the defect structure, but no ^{31}P. There is the formation of one aggregate defect having trigonal symmetry involving substitutional Au or Pt and three interstitial Li ions and the formation of one defect with orthorhombic symmetry involving substitutional Au or Pt and one interstitial Li ion.

This paper describes the experimental results, to which a brief discussion of the microscopic defect structures and the hfi is added. The nature of the bonding between Li and Au_{Si} (Pt_{Si}), as well as the electronic structure of these four aggregate defects, is discussed in part II of the paper (see following article Ref. 10).

II. EXPERIMENTAL DETAILS

A. Sample preparation

Into single crystals of Si, either grown by the Czochralsky method or by the float-zone technique, Au, Pt, and Li were diffused. Details of the diffusion, annealing, and quenching processes were described by Höhne[4] and are not repeated here. The Au-Li and Pt-Li aggregate defects were detected in Si, which was originally n type (P doping) or p type (B doping). However, the samples were not very homogeneous.

0163-1829/95/52(7)/4998(9)/$06.00

B. EPR and ENDOR measurements

EPR and ENDOR measurements were performed with custom-built computer-controlled X- and K-band spectrometers working at 9.45 GHz and 24.6 GHz, respectively. The stationary ENDOR method was used (see, e.g., Ref. 11). The samples were placed in a cylindrical cavity, which contained four vertical rods as two Helmholtz coils for the rf radiation for ENDOR and worked in the TE_{011} mode. The temperature of the samples could be varied between 3.4 K and room temperature. The ENDOR frequency was varied between 0.3 and 200 MHz. The samples could be illuminated *in situ*. The ENDOR signals were processed using digital filters and a peak search algorithm.

III. EXPERIMENTAL RESULTS

A. EPR measurements

Figures 1(a)–(d) shows the angular dependencies of the EPR spectra for rotation of the magnetic field in a {110} plane. The spectra in Figs. 1(a) and (b) clearly display trigonal symmetry, those of Figs. 1(c) and (d) orthorhombic symmetry. The centers of the measured hf split line groups are indicated as experimental points. A small misalignment of the crystals in the cavity results in the splitting of two degenerate defect orientations [Figs. 1(b)–(d)]. The solid lines are the calculated angular dependencies using the appropriate spin Hamiltonian [see Eq. (1) below]. The resulting g matrices are given in Table I.

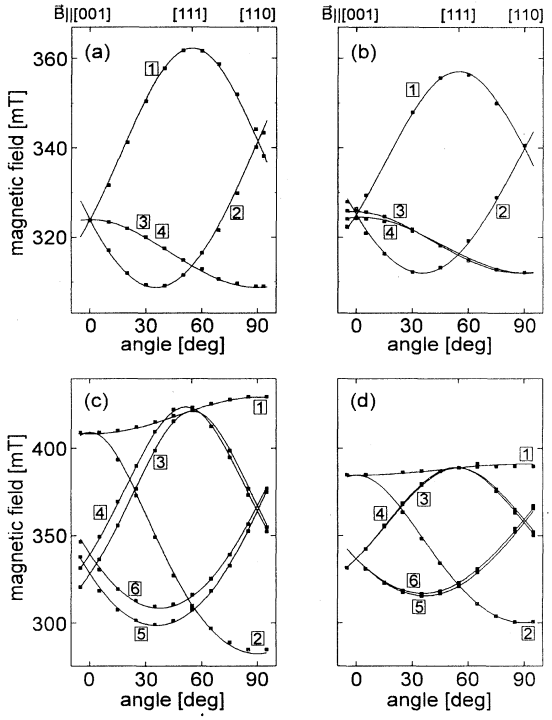

FIG. 1. EPR angular dependencies of the trigonal and orthorhombic Au (Pt)-Li aggregate defects for rotation of the magnetic field in the (110) plane (X band). A small misalignment of the crystal in the cavity lifts the degeneracy of two defect orientations. The squares are the experimental centers of the hf structures. The solid lines are calculated with the g matrices of Table I. The numbers in squares denote the four and six center orientations, respectively. (a) Trigonal Au-Li defect, measured at 8 K after illumination; (b) trigonal Pt-Li defect, measured at 8 K; (c) orthorhombic Au-Li defect, measured at 4 K; (d) orthorhombic Pt-Li defect, measured at 4 K.

In Fig. 2, characteristic spectra show the splittings due to the hfi with Au, Pt, and Si for the two trigonal and the two orthorhombic defects. The number of hf split lines and their intensities are in agreement with the nuclear spins of the involved isotopes and their respective natural abundancies: ^{29}Si ($I = 1/2, 4.7\%$), ^{197}Au ($I = 3/2, 100\%$), and ^{195}Pt ($I = 1/2$, 33.8%). The other isotopes of Si and Pt have $I = 0$. The hf lines of Au (Pt) are indicated by the upper arrows in Fig. 2, while those of ^{29}Si are indicated by the lower arrows. The Au hf splitting of the orthorhombic Au-Li aggregates could only be resolved at magnetic fields larger than 360 mT and with very low magnetic field modulation amplitudes, which were too small for the simultaneous observation of the Si hf structure.

If the field modulation amplitude is sufficiently high to see the ^{29}Si hf structure clearly (Fig. 3), the Au hf structure is no longer resolved. The assignment of the quartet hf structure to ^{197}Au and not to ^{7}Li, which also has $I = 3/2$, is verified by ENDOR experiments (see below).

The spectra show clearly that each of the defects con-

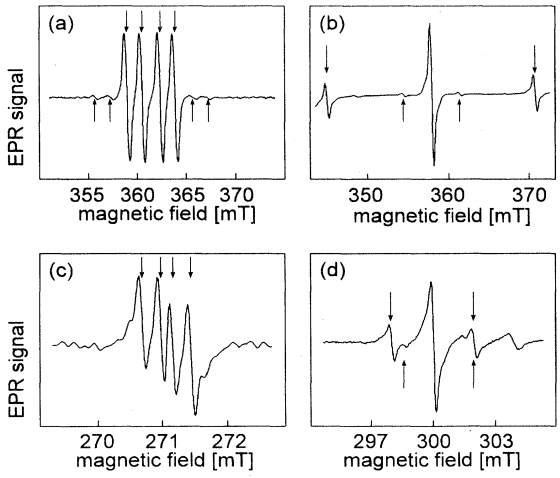

FIG. 2. Hf structure of the trigonal and orthorhombic Au (Pt)-Li aggregate defects. The upper arrows indicate ^{197}Au (^{195}Pt) hf split lines, the lower arrows the hf split ^{29}Si lines (X band). (a) Trigonal Au-Li defect, center orientation 1 in Fig. 1(a), $B \parallel [111]$, $T = 8$ K; (b) trigonal Pt-Li defect, center orientation 1 in Fig. 1(b), $B \parallel [111]$, $T = 8$ K; (c) orthorhombic Au-Li defect, center orientation 2 in Fig. 1(c), $B \parallel [110]$, $T = 4$ K; (d) orthorhombic Pt-Li defect, center orientation 2 in Fig. 1(d), $B \parallel [110]$, $T = 4$ K.

TABLE I. Experimental g matrices, hf and quadrupole interactions of four Au (Pt)-Li aggregate defects in Si. The angles in row 4 and 5 give the orientation of the principal directions of the Li hf and quadrupole matrices. The absolute signs of the hfi are unknown. For the hfi constants measured with ENDOR (a, b, b', and q), relative signs could be determined.

	Au-Li	Pt-Li	$Au\text{-}Li_3$	$Pt\text{-}Li_3$
symmetry	orthorhombic	orthorhombic	trigonal	trigonal
S	1/2	1/2	1/2	1/2
g	$g_{\parallel[\bar{1}10]} = 2.456$ $g_{\parallel[110]} = 1.548$ $g_{\parallel[001]} = 1.629$	$g_{\parallel[\bar{1}10]} = 2.250$ $g_{\parallel[110]} = 1.746$ $g_{\parallel[001]} = 1.769$	$g_{\parallel[111]} = 1.852$ $g_{\perp[111]} = 2.214$	$g_{\parallel[111]} = 1.898$ $g_{\perp[111]} = 2.165$
$A_{Au/Pt}$	$\lvert A_{\parallel[\bar{1}10]}/h\rvert \approx 8.5$ MHz $\lvert A_{\parallel[110]}/h\rvert \approx 0$ MHz $\lvert A_{\parallel[001]}/h\rvert \approx 0$ MHz	$\lvert A_{\parallel[\bar{1}10]}/h\rvert = 118$ MHz $\lvert A_{\parallel[110]}/h\rvert = 247$ MHz $\lvert A_{\parallel[001]}/h\rvert = 134$ MHz	$A_{\perp[111]}/h = 36.3$ MHz $A_{\parallel[111]}/h = 51.7$ MHz	$\lvert A_{\perp[111]}/h\rvert = 321$ MHz $\lvert A_{\parallel[111]}/h\rvert = 696$ MHz
Q_{Au}	$Q_{\parallel[110]}/h \approx 1.4$ MHz		$Q_{\parallel[111]} = -2Q_{\perp[111]}$ $Q_{\parallel[111]}/h > 80$ MHz	
A_{Li}	$a/h = 0.861$ MHz $b/h = 0.398$ MHz $b'/h = -0.730$ MHz $x \parallel [110]$ $y \parallel [\bar{1}10]$ $z \parallel [001]$	$A_{\parallel[110]} = 0.42$ MHz	$a/h = -0.095$ MHz $b/h = 0.494$ MHz $b'/h = 0.103$ MHz $\triangle/h = 1.330$ MHz $\angle(x,[001]) = 58°$ $y \parallel [1\bar{1}0]$ $\angle(z,[001]) = 148°$	$a/h = 1.285$ MHz $b/h = 0.604$ MHz $b'/h = 0.289$ MHz $\triangle/h = 1.710$ MHz $\angle(x,[001]) = 50°$ $y \parallel [1\bar{1}0]$ $\angle(z,[001]) = 140°$
Q_{Li}	$q/h < 10$ kHz		$q/h = 9.6$ kHz $q'/h = 2.1$ kHz $x \parallel [1\bar{1}0]$ $\angle(y,[001]) = 210°$ $\angle(z,[001]) = 120°$	$q/h = 13.4$ kHz $q'/h = 0.7$ kHz $x \parallel [1\bar{1}0]$ $\angle(y,[001]) = 211°$ $\angle(z,[001]) = 121°$
A_{Si}	$A_{\parallel[\bar{1}10]}/h = -107$ MHz $A_{\parallel[110]}/h = -106$ MHz $A_{\parallel[001]}/h = -128$ MHz	$A_{\parallel[\bar{1}10]}/h = -88$ MHz $A_{\parallel[110]}/h = -96$ MHz $A_{\parallel[001]}/h = -71$ MHz	$A_{\perp[111]}/h = -129$ MHz $A_{\parallel[111]}/h = -196$ MHz	$A_{\perp[111]}/h = -153$ MHz $A_{\parallel[111]}/h = -192$ MHz

tains either a single Au or a single Pt atom. The resolved Si hf structure of the trigonal defects is due to the interaction with a single Si atom on the trigonal axis,[4,5] that of the two orthorhombic defects due to the interaction with two Si atoms, which are equivalent within experimental error. This follows from the intensity ratios of the Au (Pt) lines to the ^{29}Si lines. The Si hf splitting of the orthorhombic centers has a low anisotropy.

The EPR and ENDOR spectra are described by an effective spin $\mathcal{S} = 1/2$, because neither in EPR[4,5] nor in ENDOR spectra was there an indication for a higher effective spin. We, therefore, use the following spin Hamiltonian (with $\mathcal{S} = 1/2$) to fit the spectra,

$$\mathcal{H} = \mu_B \mathbf{B} \cdot \underline{g} \cdot \boldsymbol{\mathcal{S}} + \sum_k \Big(\mathbf{I}_k \cdot \underline{A}_k \cdot \boldsymbol{\mathcal{S}} - g_{n,k}\mu_n \mathbf{B} \cdot \mathbf{I}_k + \mathbf{I}_k \cdot \underline{Q}_k \cdot \mathbf{I}_k \Big). \quad (1)$$

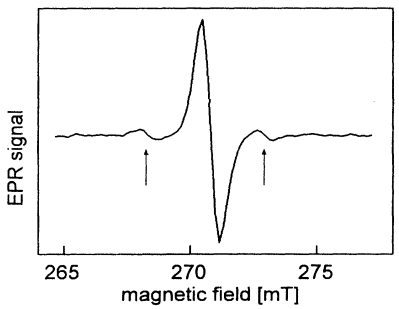

FIG. 3. ^{29}Si hf structure of the orthorhombic Au-Li defect for $B \parallel [110]$. Because of the large magnetic field modulation amplitude, the Au hf structure is not resolved.

The symbols have their usual meaning,[11] the summation includes all nuclei for which we have resolved interactions. The principal values of the $\underline{g}$, $\underline{A}$, and $\underline{Q}$ matrices determined from the EPR spectra are listed in Table I. From the EPR spectra, only approximate values for the

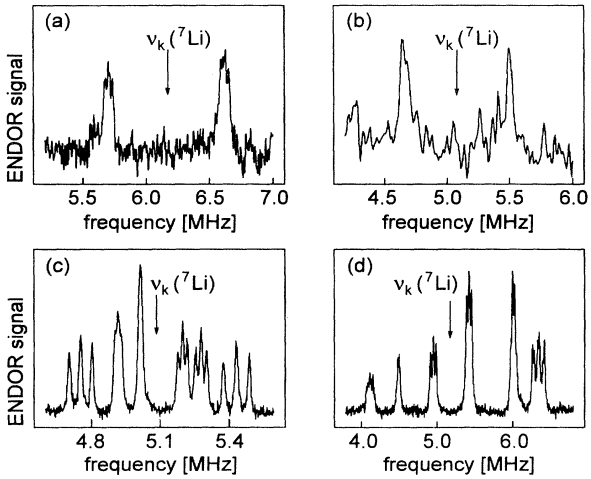

FIG. 4. ^{7}Li ENDOR spectra of the trigonal and orthorhombic Au (Pt)-Li defects. The arrows denote the Larmor frequency of the ^{7}Li nuclei. (a) Orthorhombic Au-Li defect, center orientation 2 in Fig. 1(c), measured at 3.4 K; $B \parallel [110]$; (b) orthorhombic Pt-Li defect, center orientation 2 in Fig. 1(d), measured at 4.2 K; $B \parallel [110]$; (c) trigonal Au-Li defect, center orientations 3 and 4 in Fig. 1(a), measured at 8.7 K; $B \parallel ([001] + 63°)$, $B \perp [1\bar{1}0]$; (d) trigonal Pt-Li defect, center orientations 3 and 4 in Fig. 1(b), measured at 12.7 K; $B \parallel ([001] + 75°)$, $B \perp [1\bar{1}0]$.

quadrupole interaction of Au could be determined.

The EPR of the trigonal Au-Li aggregates was only detected during and after illumination with light. (A photon energy of 0.5 eV is sufficient for the detection. The largest signal is obtained when illuminating with near-band-gap light.) This has already been noted by Höhne.[4] The EPR signals vanished after warming the crystal to 160 K and cooling down again in the dark. Illumination with white light increased the EPR signal intensity of the orthorhombic Pt defects, but had no influence on the orthorhombic Au-Li and on the trigonal Pt-Li aggregates.

The EPR signals of the trigonal and orthorhombic Au defects show different, almost contrary, temperature dependencies. While the trigonal centers have their largest signals at temperatures around 10 K, which become weaker towards lower temperatures and almost vanish at 4 K because of saturation effects, the signals of the orthorhombic centers increase when lowering the temperature. At first sight, this may suggest a thermal bistability. However, the ratio of the EPR signal intensities at a given temperature varies from sample to sample. Thus, a thermal bistability could be excluded. The ENDOR experiments, discussed below, confirm this.

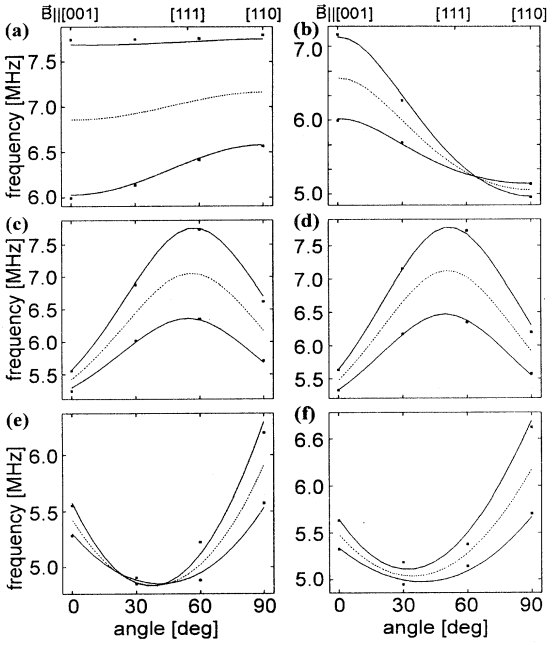

FIG. 5. Angular dependence of the ^{7}Li ENDOR lines for all six center orientations of the orthorhombic Au-Li defect [see Fig. 1(c)]. The magnetic field was rotated in the (110) plane at 3.4 K. The solid lines were calculated using the hfi parameters of Table I, the dotted lines represent the field dependence of the ^{7}Li Larmor frequencies. (a) through (f) are for orientations 1–6, respectively.

B. ^{7}Li ENDOR measurements

1. ENDOR spectra and angular dependencies

The participation of Li in these four defects was not revealed by EPR, because the Li hfi are very small. However, ENDOR experiments were successful. Figure 4 shows ^{7}Li ENDOR spectra for all four defects. The signal-to-noise ratio of the ENDOR lines of the orthorhombic defects is smaller than that of the trigonal ones. The EPR of these centers could not be saturated as well as those of the trigonal centers at the lowest temperature attainable in our spectrometer (3.4 K).

In all four defects, the centers of the ENDOR line groups coincide with the Larmor frequency of ^{7}Li. This already shows, together with the detailed analysis of the angular dependence of the spectra, that the lines are due to ^{7}Li (see also Ref. 11). Thus, in all four defects, Li is involved as part of the defect structure.

The orthorhombic centers have two ^{7}Li lines, which result from NMR transitions in the two states $m_S = \pm 1/2$. Since I (^{7}Li) = 3/2, a quadrupole splitting could have been expected. However, no quadrupole splitting is resolved. From the linewidth (approximately 100 kHz half width), an upper limit of the nuclear quadrupole interaction can be estimated to be 10 kHz.

The angular dependencies of the ENDOR frequencies of the orthorhombic Au-Li defect are shown in Fig. 5 for rotation of the magnetic field in a {110} plane. The ENDOR angular dependencies were measured for all six center orientations, which are indicated in Fig. 1(c). For each orientation of the magnetic field with respect to the crystal axes, the magnetic field value was adjusted to the EPR resonance positions [according to Fig. 1(c)] "following" the EPR lines of each center orientation. The angular dependencies show that only one Li atom is involved in the orthorhombic defects, which is located on the orthorhombic axis (⟨100⟩ axes): Had there been more Li atoms or lower symmetry sites for the Li atoms, we would have seen more ENDOR lines. Thus, the orthorhombic defect is identified as an Au (Pt)-Li pair. The ^{7}Li hf and quadrupole interaction constants determined from the analysis of the angular dependencies of the ENDOR frequencies are listed in Table I. The signal-to-noise ratio of the ^{7}Li ENDOR lines of the orthorhombic Pt-Li pair defect for orientations outside $B_0 \parallel [110]$ was not sufficient for the measurement of their angular dependence. Therefore, in Table I, only the hfi for $B \parallel [110]$ could be given.

In contrast to the orthorhombic defects, the ^{7}Li ENDOR spectra of the trigonal defects consist of six triplets [Figs. 4(c), (d)]. Figure 6 shows the ENDOR angular dependence for one of the four trigonal defect orientations [labeled as 1 in Figs. 1(a), (b)]. The quadrupole interaction with ^{7}Li is responsible for the resolved triplet structure: the three lines belong to the transitions $m_I = -3/2 \leftrightarrow m_I = -1/2$, $m_I = -1/2 \leftrightarrow m_I = 1/2$, and $m_I = 1/2 \leftrightarrow m_I = 3/2$. Two such triplets would be expected for one Li atom on the trigonal axis. Since six triplets are observed, there are three different Li sites for one single trigonal defect orientation (for each m_S value, there are two ENDOR triplets: thus, three Li ligands have six ENDOR triplets). Furthermore, each of these Li sites must be in a {110} mirror plane also containing the Au

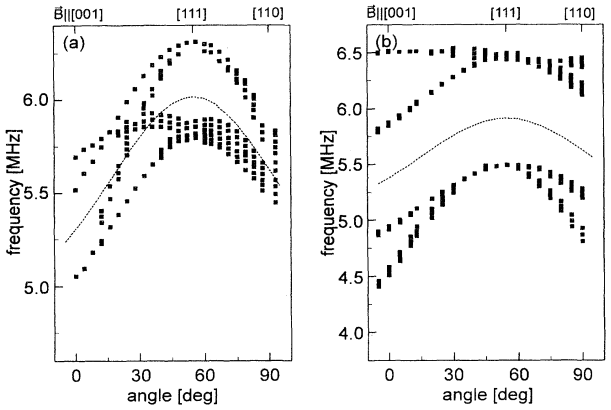

FIG. 6. Angular dependencies of the ^{7}Li ENDOR lines of the trigonal Au (Pt)-Li defects for rotation of the magnetic field in the (110) plane. The dotted lines represent the field dependence of the ^{7}Li Larmor frequencies, the squares the experimental line positions. (a) Trigonal Au-Li defect of orientation 1 of Fig. 1(a), measured at 8.7 K; (b) trigonal Pt-Li defect of orientation 1 of Fig. 1(b), measured at 12.7 K.

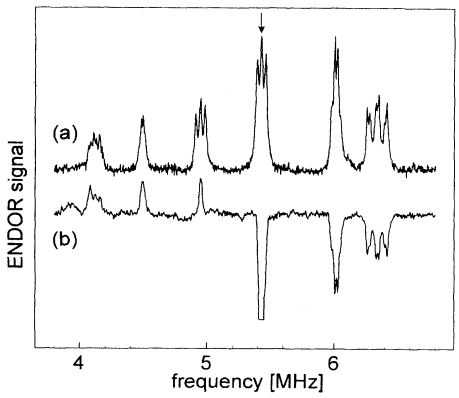

FIG. 7. ^{7}Li ENDOR and ^{7}Li double-ENDOR spectra of the trigonal Pt-Li defect for $B \parallel ([001] + 75°), B \perp [1\bar{1}0]$, 313 mT trace (a) ENDOR spectrum, trace (b) double-ENDOR spectrum with the monitor line at 5.41 MHz (arrow).

(Pt) atom. If the Li ligand had occupied a site with lower symmetry, more Li ENDOR triplets would have been observed. If Li, e.g., had not been on the mirror planes, one would have seen twelve ENDOR triplets, because of the mirroring at these planes.

At this point, one cannot decide whether these three sites are simultaneously occupied [Au_{Si}-Li_3 (Pt_{Si}-Li_3) structure], or whether only one site at a time, which means that three differently oriented Au-Li pairs of lower, monoclinic symmetry are observed. For both cases, one would observe the same ENDOR spectra and ENDOR angular dependencies, since, in the case of monoclinic Au (Pt)-Li pairs, one would always measure the superposition of all these pairs. Strictly speaking, if only one Li belonged to the defect, there would not be a trigonal symmetry anymore. However, if this Li interacts only very weakly with the unpaired electron, then this lowering of symmetry is not necessarily seen in the EPR spectra, nor in the ENDOR spectra. This question is also relevant for the exclusion of a possible bistability between the orthorhombic and "trigonal" pairs.

Therefore, an experiment is needed with which it can be decided how many Li ligands belong to one "trigonal" defect. For this purpose, we performed double-ENDOR experiments, in which two NMR transitions are induced simultaneously. If both nuclei belong to the same defect, the NMR transitions both influence the desaturation of the partly saturated EPR of the unpaired electron, which results in a mutual influence of the two ENDOR lines. This can be detected with a double lock-in technique (for details and examples see, e.g., Ref. 11). A double-ENDOR signal is observed if the two nuclei belong to the same defect. It is not seen if the two nuclei are coupled to different defects, or — for anisotropic g factors — to different orientations of the same defect.

In our double-ENDOR experiment, the change of the ENDOR signal intensity of one ^{7}Li ENDOR transition at a fixed frequency (so-called monitor line) is observed as a function of the frequency of a second rf radiation, which is swept through the range where the other Li ENDOR lines appear. In this experiment, it must be assured that the crystal orientation with respect to the magnetic field is chosen such that the ENDOR lines of two different defect orientations are not superimposed. Figure 7, trace (b), shows the ^{7}Li double-ENDOR spectrum measured for the Pt-Li aggregate when using the line at 5.41 MHz as monitor line for a field orientation perpendicular to a $\langle 110 \rangle$ direction in comparison to the ENDOR spectrum for the same orientation [trace (a)]. Since lines of all six Li triplets appear in the double-ENDOR spectrum, this shows that all lines belong to one defect in a single center orientation. This proves that each trigonal center has three Li ligands. The monitor line belongs to $m_S = -1/2$, the double-ENDOR lines with the same sign, too, while those with the opposite sign are due to the other m_S state (so-called "special triple resonance," see, e.g., Ref. 11). Note, that the two quadrupole lines at 5 MHz are missing in the double-ENDOR spectrum. This is probably due to some relaxation mechanism.

Thus, we have established that the trigonal centers are Au_{Si}-Li_3 (Pt_{Si}-Li_3) aggregate defects. We have detected two different stages of the Li aggregation: One with one Li and one with three Li ligands. Apparently, the stage with two Li ligands is not observable.

2. *Quantitative analysis of the ^{7}Li ENDOR spectra*

The ENDOR spectra of the orthorhombic Au-Li defects are analyzed with $S = 1/2$ by diagonalizing the spin Hamiltonian Eq. (1) numerically. The results are listed in Table I in terms of the isotropic hf constant a, and the anisotropic hf constants b and b', which are related to the principal values of the usual hf matrix by

$$A_{xx} = a - b + b', \quad A_{yy} = a - b - b', \quad A_{zz} = a + 2b. \tag{2}$$

The quadrupole interaction constants q and q' are related to the principal values of the quadrupole matrix by

$$Q_{xx} = -q + q', \quad Q_{yy} = -q - q', \quad Q_{zz} = 2q. \tag{3}$$

Again, the experimental data for the orthorhombic Pt-Li defects were not sufficient for a full analysis (see above). However, a difficulty arose, when we followed the usual procedure to fit the ^{7}Li ENDOR spectra of the Au-Li$_3$ and Pt-Li$_3$ defects. This is demonstrated in Fig. 8, where the ^{7}Li ENDOR angular dependence of the trigonal center of orientation 3 [see Fig. 1(b)] is shown for the Pt-Li$_3$ defect. It was not possible to fit the angular dependence of both states $m_S = \pm 1/2$ with the same set of hfi constants and matrix orientations, satisfactorily.

If we fit the ENDOR angular dependence of the lines of one m_S state [$m_S = -1/2$ in Fig. 8(a), and $m_S = +1/2$ in Fig. 8(b)], the lines corresponding to the other m_S state are represented poorly. The attempt of a simultaneous fit fails, too [Fig. 8(c)]. In principle, there are two possibilities to overcome these difficulties: One can either try to use an anisotropic nuclear g-matrix $g_{n,\mathrm{Li}}$ or an asymmetric hf matrix $\underline{A}^{\mathrm{Li}}$. To test which possibility can be ruled out we additionally performed ENDOR experiments in a K-band spectrometer ($\nu_{\mathrm{EPR}} \approx 24.6$ GHz). If we use an anisotropic nuclear $g_{n,\mathrm{Li}}$ matrix, we are not able to fit both ENDOR spectra (K band and X band) with the same set of parameters. The use of an asymmetric hf matrix is successful.

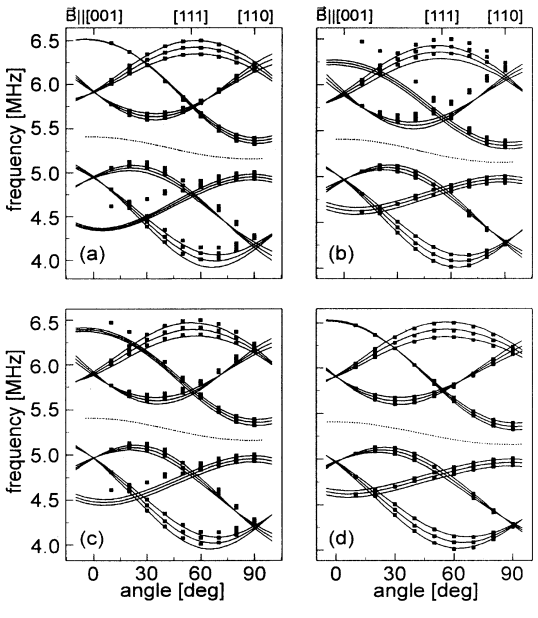

FIG. 8. Experimental (X-band) ^{7}Li ENDOR angular dependence of the trigonal Pt-Li defects (squares) fitted to symmetrical [(a)–(c)] and an asymmetric hf matrix (d). In (a) the interaction parameters were adjusted to fit the m_S=-1/2 lines, in (b) to fit the m_S=+1/2, and in (c) it was attempted to fit both $m_S = \pm 1/2$ spectra with one symmetrical hf matrix. A satisfactory description requires an asymmetry parameter (d) (see Table I).

Usually, it is assumed that hf matrices are symmetric. Although the hf matrices for defects with low symmetry will generally have nine independent elements and will not necessarily be symmetric, there are only very few reports on asymmetric hf matrices until now[12–14] (to the best of our knowledge).

The symmetry constraints of the hf matrix are determined by the subgroup of elements of the point group describing the defect symmetry, which contains all symmetry operations that leave invariant the positions of the defect atoms and of the nucleus causing the hfi. Since the hf matrix has to be invariant under all symmetry operations of the subgroup, one can determine the number of independent hf matrix elements. When the subgroup describes monoclinic or "no symmetry" (C_1), in principle, nine independent matrix elements have to be determined (and the hf matrix is not necessarily symmetric).

In our case, the symmetry for the Li ligands is monoclinic. We obtain a perfect fit (within experimental error) if we use one asymmetry parameter $\triangle = (A_{xz} - A_{zx})/2$. [The y direction is perpendicular to the (110) mirror plane, the z and x directions are in the mirror plane.] The ^{7}Li hf matrix can be noted as

$$\underline{A}_{\mathrm{Li}} = \underbrace{\begin{pmatrix} a-b+b' & & \\ & a-b-b' & \\ & & a+2b \end{pmatrix}}_{\text{symmetric part}} + \underbrace{\begin{pmatrix} 0 & 0 & -\triangle \\ 0 & 0 & 0 \\ \triangle & 0 & 0 \end{pmatrix}}_{\text{asymmetric part}}. \tag{4}$$

Figures 8(d) and 9 show the simultaneous fits of lines corresponding to both states $m_S = \pm 1/2$ in the X band and K band, respectively. In both bands, there is now excellent agreement between experiment and calculation. The resulting interaction parameters are given in Table I.

C. ^{197}Au ENDOR spectra

^{197}Au ENDOR spectra could be measured for the $m_I = 1/2 \leftrightarrow m_I = -1/2$ NMR transitions of the trigonal defect. Figure 10 shows their angular dependence. The two ENDOR lines for $m_I = \pm 1/2$ were detected. The hf matrix of ^{197}Au turned out to be axially symmetric about the ⟨111⟩ directions. The isotropic hfi constant is about a factor of 10 higher than the anisotropic one. From the analysis of the EPR spectra a quadrupole interaction parameter of $q/h \approx 20$ MHz was expected.[4] However, in the appropriate frequency range no other ^{197}Au lines were found, none up to 200 MHz. We must, therefore, conclude that $|q/h|$ exceeds 40 MHz. The hfi constants are listed in Table I.

No ^{197}Au ENDOR lines could be observed for the or-

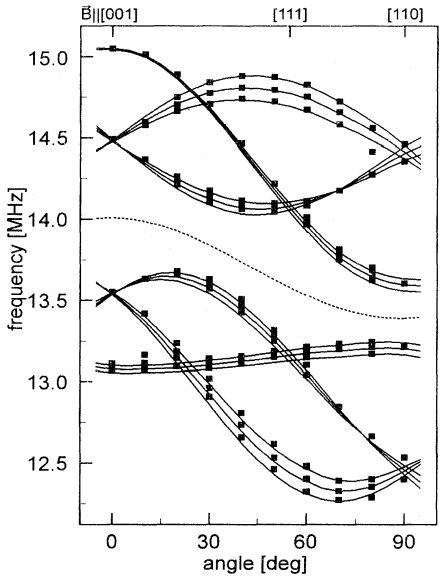

FIG. 9. Experimental ^{7}Li ENDOR angular dependence for trigonal Pt-Li defects measured in K band (squares) and calculated angular dependence using the asymmetric hf matrix of Table I.

thorhombic defect, only ^{7}Li lines. Nor could any ^{195}Pt lines be seen of the orthorhombic Pt-Li pair defect. In the trigonal Pt-Li_3 defects, the ^{195}Pt interaction, well resolved in EPR, is too large for the available ENDOR frequency range. Their ^{195}Pt lines would be beyond 200 MHz.

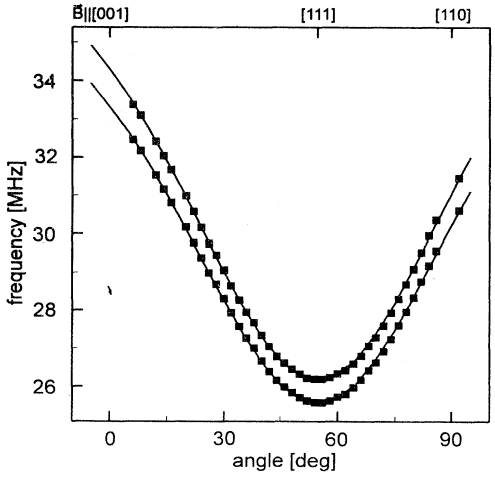

FIG. 10. Experimental ^{197}Au ENDOR angular dependence for the trigonal Au-Li defect in center orientation 1 in Fig. 1(a), measured in X band (squares) and calculated angular dependence using the hf matrix of Table I.

D. ^{29}Si ENDOR spectra

^{29}Si ENDOR lines were only observed for the trigonal defects. They were investigated in detail for the Pt-Li_3 defect. Because of the low natural abundance of ^{29}Si (4.7%), the signal-to-noise ratio was much smaller than that of the ^{7}Li lines (abundance 92.5%) and long integration times were necessary. Figure 11 gives an example for the spectra and shows the weak ^{29}Si lines in comparison to the ^{7}Li lines. The largest Si hfi was already resolved in the EPR spectrum.[5] The ENDOR investigation confirmed that this ^{29}Si interaction is axially symmetric about a $\langle 111 \rangle$ direction and due to one ^{29}Si ligand. In Table II, the shf interaction constants and matrix orientations of 15 shells of ^{29}Si ligands are listed for the Pt-Li_3 defect.

IV. DISCUSSION

From the analysis of the ENDOR experiments, we know that both the trigonal and orthorhombic Au (Pt) related defects are aggregate defects involving three and one Li ligand, respectively. From the EPR spectra, it is also clear that one paramagnetic Au and Pt atom, respectively, is involved in the defects. Paramagnetic substitutional Pt is known from EPR investigations[15,16] to be Pt_{Si}^{-}, a defect with the same C_{2v} symmetry as the orthorhombic Pt-Li aggregate investigated here. The Pt hfi is of the same order of magnitude (about a factor of two larger) and the hfi with the two nearest ^{29}Si ligands are very similar to those found for the orthorhombic Pt-Li pair defect. We, thus, conclude that in the orthorhombic Pt-Li pair defect Pt is substitutional as Pt_{Si}^{-}. In the orthorhombic Au-Li pair, we assume that instead of Pt_{Si}^{-}, there is Au_{Si}^{0}. From ENDOR, we concluded that one Li ligand must be on the orthorhombic axis, which is the intersection line of two {110} mirror planes: a $\langle 001 \rangle$ di-

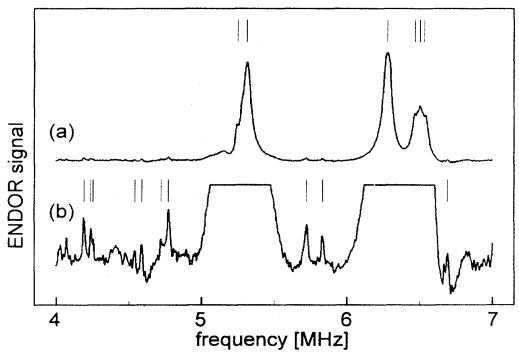

FIG. 11. ^{29}Si and ^{7}Li ENDOR lines of the trigonal Pt-Li defect for $B \parallel ([001]+30°)$, $B \perp [1\bar{1}0]$, $B = 348$ mT, $T = 12.7$ K. Trace (a): the vertical bars indicate the ^{7}Li lines, the ^{29}Si lines are hardly seen. Trace (b): amplification of spectrum (a) by a factor of 30. The ^{29}Si lines are now visible, the Li lines were truncated.

TABLE II. Experimental ^{29}Si hfi. The angles Θ, Ψ, Φ are the Euler angles describing the orientation of the principal axes (x, y, z) of the hf matrix relative to the crystal system ([100], [010], [001]). Θ is the angle between the z axis of the matrix and the [001] crystal direction. s is defined as the line of intersection of the xy plane with the (001) plane, where the positive direction is chosen in a way, that z, [001] and s form a right hand system. Then Ψ is defined as the angle between the x axis and s, Φ as the angle between s and the [100] direction.

Symmetry type	Number of nuclei	a/h [MHz]	b/h [MHz]	b'/h [MHz]	
Trigonal	1	165.3	13.0		$z \parallel [111]$
Monoclinic	3	35.0	3.24	0.91	$\Theta = 61°$, $\Psi = 0°$, $\Phi = 45°$
Monoclinic	3	21.7	2.58	0.09	$\Theta = 53°$, $\Psi = 0°$, $\Phi = 45°$
Triclinic	6	24.7	2.10	0.46	$\Theta = 142°$, $\Psi = -5°$, $\Phi = 37°$
Monoclinic	3	7.04	0.94	0.13	$\Theta = 74°$, $\Psi = 0°$, $\Phi = 45°$
Triclinic	6	3.34	0.57	0.32	$\Theta = 135°$, $\Psi = 90°$, $\Phi = 57°$
Monoclinic	3	3.06	0.39	0.04	$\Theta = 58°$, $\Psi = 0°$, $\Phi = 45°$
Trigonal	1	1.39	0.23		$z \parallel [111]$
Triclinic	6	2.20	0.21	0.18	$\Theta = 77°$, $\Psi = 27°$, $\Phi = 36°$
Monoclinic	3	1.68	0.16	0.04	$\Theta = 123°$, $\Psi = 0°$, $\Phi = 45°$
Monoclinic	3	1.22	0.15	0.12	$\Theta = 150°$, $\Psi = 90°$, $\Phi = 45°$
Monoclinic	3	1.73	0.08	0.02	$\Theta = 2°$, $\Psi = 0°$, $\Phi = 45°$
?		−1.06	0.06	<0.02	$z \approx \parallel [111]$
?		0.88	0.05	<0.02	$z \approx \parallel [111]$
?		−0.82	0.02	<0.02	$z \approx \parallel [111]$

rection. Thus, a model, as the one shown in Fig. 12(a), is proposed for the orthorhombic defects, in which Li occupies an interstitial position.

For the trigonal centers it was established by ENDOR that three Li ligands must be arranged with trigonal symmetry about a ⟨111⟩ trigonal axis. We propose a model with three interstitial Li ligands along ⟨111⟩ directions in an arrangement as the one shown in Fig. 12(b).

In part II of the paper a detailed discussion of the electronic structure of these aggregate defects is presented.[10] Here, only a few qualitative arguments on the electronic structure are discussed.

The Li ligands must be largely ionic. Isolated Li^0 is paramagnetic and a very shallow donor. Combined with Pt^- or Au^0 it would transfer its outer electron to the deep state of the noble metals. The order of magnitude of the anisotropic hfi can be explained by the classical point-dipole-dipole interaction between the unpaired electron at the Au^0 (Pt^-) atom and the interstitial Li^+ ligands. The point dipole of a full unpaired electron on Au^0 (Pt^-) would cause a value of $b/h = 1.5$ MHz at the Li^+ along [001] 2.72 Å away from the center (orthorhombic defect) and $b/h = 2.3$ MHz along ⟨111⟩ 2.35 Å away from the center of the trigonal defect. Considering, that only a fraction of 0.1–0.2 of an unpaired electron is localized at the centers, which can be estimated from the Au (Pt) hfi [see also part II, Ref. 10], it is clear that the hfi of Li^+ can be qualitatively understood in an ionic model. Thus, we think that Li^+ is aggregated to Au^0 (Pt^-) by means of an ionic bonding, forming neutral orthorhombic Pt^--Li^+ aggregates and positive orthorhombic Au^0-Li^+ aggregates. In the case of the trigonal centers, the three Li atoms deliver three electrons to the defect, which would result in the formal charges of Pt^{3-} and Au^{2-}, respectively [see Fig. 12(b)]. For a detailed discussion of the charge density, see part II Ref. 10.

From the experiment it is not possible to assign specific ligands to the measured ^{29}Si hfi matrices without having a detailed theory of the electronic structure. This is a well-known difficulty for ENDOR studies of point

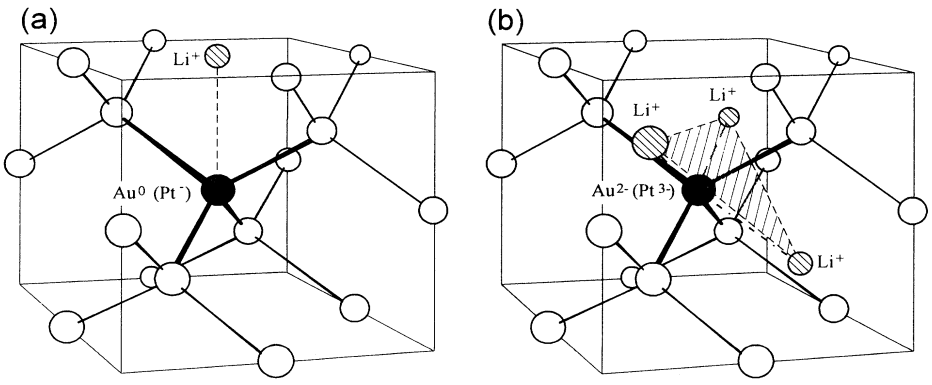

FIG. 12. Proposed models for the orthorhombic Au (Pt) - Li defects (a) and the trigonal Au (Pt)-Li defects (b).

defects in Si. The largest Si interaction belongs to a substitutional nearest neighbor Si as will be shown in part II of this paper.[10] For four monoclinic ^{29}Si ligands the hfi matrix orientations, where the hfi is largest, point almost into ⟨111⟩ orientations. There are no Si ligands for which the large hfi points along the cubic axes. This is an observation usually made for substitutional impurity centers, such as, for example, the chalcogens S^+, Se^+, and Te^+ and also for vacancy related centers (e.g., negative Si vacancy, the oxygen-vacancy complex).[17–21] On the other hand, interstitial impurities, such as Fe_i^0, have large interactions along the ⟨001⟩ directions.[22] Thus, our observation is in line with the assignment of Au and Pt being on substitutional sites. In part II, the spin densities at the Si ligands are calculated and compared with the experiment.[10]

V. CONCLUSION

We have shown with a detailed ENDOR investigation that, upon Li diffusion into Si containing Au or Pt, Li^+ aggregates in two ways with substitutional Pt or Au: it forms an orthorhombic pair defect, in which Li^+ is on an interstitial site along a ⟨001⟩ direction, and it forms a trigonal defect, in which three Li^+ ions occupy interstitial sites along ⟨111⟩ directions. No aggregates with only two Li^+ ions were found. It seems from our observations that Li cannot passivate substitutional Au^0 (Pt^-) defects in Si, but simply forms new, electrically active, aggregate centers.

[1] M. Höhne, Phys. Status Solidi B **99**, 651 (1980).
[2] R. L. Kleinhenz, Y. H. Lee, J. W. Corbett, E. G. Sieverts, S. H. Muller, and C. A. J. Ammerlaan, Phys. Status Solidi B **108**, 363 (1981).
[3] H. H. Woodbury and G. W. Ludwig, Phys. Rev. **117**, 1287 (1960).
[4] M. Höhne, Phys. Status Solidi B **138**, 337 (1986).
[5] M. Höhne, Phys. Status Solidi B **156**, 325 (1989).
[6] A. Chantre and D. Bois, Phys. Rev. B **31**, 7979 (1985).
[7] J. J. van Kooten, G. A. Weller, and C. A. J. Ammerlaan, Phys. Rev. B **30**, 4564 (1984).
[8] W. Gehlhoff, K. Irmscher, and J. Kreissl, Lect. Notes Phys. **301**, 262 (1988).
[9] S. Greulich-Weber, A. Görger, J.-M. Spaeth, and H. Overhof, Appl. Phys. A **53**, 147 (1991).
[10] H. Weihrich, H. Overhof, P. Alteheld, S. Greulich-Weber, and J.-M. Spaeth, following paper, Phys. Rev. B **52**, 5007 (1995).
[11] J.-M. Spaeth, J. R. Niklas, and R. H. Bartram, in *Structural Analysis of Point Defects in Solids*, edited by Hans-Joachim Queisser, Springer Series in Solid State Sciences Vol. 43 (Springer, Berlin, 1992).
[12] V. G. Grachev, Fiz. Tverd. Tela (Leningrad) **29**, 721 (1987) [Sov. Phys. Solid State **29**, 413 (1987)].
[13] M. L. Falin, A. L. Konkin, and M. M. Zaripov, J. Phys. C **19**, 3013 (1986).
[14] P. Alteheld, Ph.D. thesis, Paderborn, Germany, 1994.
[15] H. H. Woodbury and G. W. Ludwig, Phys. Rev. **126**, 466 (1962).
[16] F. G. Anderson, R. F. Milligan, and G. D. Watkins, Phys. Rev. B **45**, 3279 (1992).
[17] J. R. Niklas and J.-M. Spaeth, Solid State Commun. **46**, 121 (1983).
[18] S. Greulich-Weber, J. R. Niklas, and J.-M. Spaeth, J. Phys. C **17** L911 (1984).
[19] S. Greulich-Weber, J. R. Niklas, and J.-M. Spaeth, J. Phys. Condens. Matter **1**, 35 (1989).
[20] M. Spenger, S. H. Muller, and C. A. J. Ammerlaan, Physica **116B**, 224 (1983).
[21] G. D. Watkins and J. W. Corbett, Phys. Rev. B **38**, 3998 (1988).
[22] S. Greulich-Weber, J. R. Niklas, E. R. Weber, and J.-M. Spaeth, Phys. Rev. B **30**, 6292 (1984).